

Testing RIAF model for Sgr A* using the size measurements

Feng Yuan^{1,2}, Zhi-Qiang Shen^{1,2} and Lei Huang^{1,3}

ABSTRACT

Recent radio observations by the VLBA at 7 and 3.5 mm produced the high-resolution images of the compact radio source located at the center of our Galaxy—Sgr A*, and detected its wavelength-dependent intrinsic sizes at the two wavelengths. This provides us with a good chance of testing previously-proposed theoretical models for Sgr A*. In this *Letter*, we calculate the size based on the radiatively inefficient accretion flow (RIAF) model proposed by Yuan, Quataert & Narayan (2003). We find that the predicted sizes after taking into account the scattering of the interstellar electrons are consistent with the observations. We further predict an image of Sgr A* at 1.3 mm which can be tested by future observations.

Subject headings: accretion, accretion disks — black hole physics — galaxies: active — Galaxy: center — radiation mechanisms: non-thermal

1. Introduction

The compact radio source located at the center of our Galaxy, Sgr A*, is perhaps the most intensively studied black hole source up to date (see review by Melia & Falcke 2001). Substantial observational results put strict constraints on theoretical models. These models include the spherical accretion model (Melia, Liu & Coker 2001; Liu & Melia 2002), the pure jet model (Falcke et al. 1993; Falcke & Markoff 2000), the advection-dominated accretion flow (ADAF) or radiatively inefficient accretion flow (RIAF) (Narayan et al. 1995; Narayan et al. 1998; Yuan, Quataert & Narayan 2003, 2004), and the coupled ADAF-jet model (Yuan, Markoff & Falcke 2002). In the present paper we concentrate on the RIAF model proposed by Yuan, Quataert & Narayan (2003, hereafter YQN03).

¹Shanghai Astronomical Observatory, Chinese Academy of Sciences, 80 Nandan Road, Shanghai 200030, China; fyuan,zshen,muduri@shao.ac.cn

²Joint Institute for Galaxy and Cosmology (JOINGC) of SHAO and USTC

³Graduate School of Chinese Academy of Sciences, Beijing 100039, China

The YQN03 model explains most of the observations available at that time, including the spectrum from radio to X-ray, the radio polarization, and the flares at both infrared and X-ray wavebands (see YQN03 for detail). After the publication of YQN03, many new observations are conducted. These include new spectral variability at millimeter wavelength (Zhao et al. 2003; Miyazaki et al. 2004; Mauerhan et al. 2005; An et al. 2005), the high angular resolution measurements of the linear polarization at submillimeter wavelengths and its variability with SMA (Marrone et al. 2005), and very high energy emissions from the direction of Sgr A* (INTEGRAL: Bélanger et al. 2004; HESS: Aharonian et al. 2004; CANGAROO: Tsuchiya et al. 2004; MAGIC: Albert et al. 2006). Several large multiwavelength campaigns have been performed (e.g., Eckart et al. 2004, 2005; Yusef-Zadeh et al. 2005). Some observations mentioned above confirm the YQN03 model, or they can be easily interpreted in the context of this model, while some observational results are not so obvious to be understood and thus offer new challenges to the model. In the present *Letter* we will discuss the size of Sgr A* at radio wavelengths, which has not been discussed in YQN03.

It has long been realized that due to the effect of scattering by the interstellar electrons, the intrinsic size of Sgr A* is only detectable at short wavelength (Davis, Walsh & Booth 1976; Lo et al. 1985, 1998; Krichbaum et al. 1997; Bower & Backer 1998). This is because the scattering theory shows that at long wavelength the observed image size will be dominated by the scattering and scale quadratically as a function of wavelength (Narayan & Goodman 1989). At short wavelength, however, precise measurements of the size of Sgr A* are seriously hampered by calibration uncertainties. Recently, great progress has been made in this aspect due to the improvement of the model fitting procedure by means of the closure amplitude. Using the VLBA, at 7 mm wavelength, Bower et al. (2004) successfully measured the size of Sgr A* of $0.712^{+0.004}_{-0.003}$ mas, Shen et al. (2005) obtained averaged size of 0.724 ± 0.001 mas and $0.21^{+0.02}_{-0.01}$ mas at 7 and 3.5 mm, respectively. By subtracting in quadrature the scattering size, they obtained an intrinsic size of 0.237 ± 0.02 mas (Bower et al. 2004) or 0.268 ± 0.025 mas (Shen et al. 2005) at 7 mm and 0.126 ± 0.017 mas at 3.5 mm (Shen et al. 2005). Since this new constraint is independent of the other observations such as spectrum and variability, it provides an independent test to investigate whether or not the RIAF model proposed by YQN03 can account for the observed sizes.

2. RIAF Model for Sgr A*

We first briefly review the RIAF model of YQN03, which can be considered as an updated version of the original ADAF model for Sgr A* (Narayan et al. 1995; 1998). Compared to the ADAF model, two main developments in the RIAF model are the inclusions of out-

flow/convection and the possible existence of nonthermal electrons. The former is based on the theoretical calculations and numerical simulations (e.g., Stone et al. 1999; Hawley & Balbus 2002). The possible existence of nonthermal electrons is due to the acceleration processes such as turbulent acceleration, reconnection, and weak shocks in accretion flow. We characterize the nonthermal population by p [$n(\gamma) \propto \gamma^{-p}$ where γ is the Lorentz factor], and a parameter η , the ratio of the energy in the power-law electrons to that in the thermal electrons. The dynamical quantities describing the accreting plasma, such as the density and temperature, are obtained by globally solving a set of accretion equations including the conservations of fluxes of mass, momentum, and energy. We assume that the accretion rate is a function of radius, i.e., $\dot{M} = \dot{M}_0(R/R_{\text{out}})^s$ (e.g., Blandford & Begelman 1999). Here R_{out} is the outer radius of the flow, i.e., the Bondi radius, \dot{M}_0 is the accretion rate at R_{out} (the Bondi accretion rate, fixed by *Chandra* observations of diffuse gas on $\sim 1''$ scales; Baganoff et al. 2003). The radiative processes we considered include synchrotron, bremsstrahlung and their Comptonization by both thermal and nonthermal electrons. The sum of the self-absorbed synchrotron radiation from the thermal electrons at different radii dominates the radio emission of Sgr A* at $\gtrsim 86$ GHz, while the radio emission at $\lesssim 86$ GHz is the sum of the synchrotron emission of both thermal and nonthermal electrons. As we stated in YQN03, there is no much freedom in the choice of parameter values in the RIAF model.

To calculate the intrinsic size of Sgr A* predicted by the RIAF model and compare with observations, we need to adjust the mass of the black hole. The mass of the black hole adopted in YQN03 is $2.5 \times 10^6 M_{\odot}$. Recent observations show that the mass should be larger— $M/M_{\odot} = 3.7 \pm 1.5, 3.3 \pm 0.6$, and $4.1 \pm 0.6 \times 10^6$ in Schödel et al. (2002, 2003), and Ghez et al. (2003), respectively. We adopt $M = 4 \times 10^6 M_{\odot}$. Thus the model parameters need to be adjusted accordingly to ensure that the adjusted model can fit the spectrum of Sgr A* equally well. The new parameters are: $\dot{M}_0 \approx 10^{-6} M_{\odot} \text{ yr}^{-1}$, $s = 0.25$, $\eta = 0.4\%$, and the fraction of the turbulent energy directly heating electrons $\delta = 0.3$. We note that the values of \dot{M}_0 , s and η change little, but the value of δ decreases from 0.55 in YQN03 to the present 0.3. This is because the electron temperature needs to decrease a bit to compensate for the increase of flux due to the increase of the mass of the black hole.

3. The size of Sgr A* predicted by the RIAF model

The observed radio morphology of Sgr A* is broadened by the interstellar scattering, which is an elliptical Gaussian along a position angle of $\sim 80^\circ$ with the major and minor axis sizes in mas of $\theta_{\text{scat}}^{\text{maj}} = (1.39 \pm 0.02)\lambda^2$ and $\theta_{\text{scat}}^{\text{min}} = (0.69 \pm 0.06)\lambda^2$, respectively (Shen et al. 2005). The observing wavelength λ is in cm. To get the intrinsic size of Sgr A*,

observers have to subtract the scattering effect from the observed image. Here, all the sizes estimated from observations are referred to as the FWHM (Full Width at Half Maximum) of the Gaussian profile. This requires that not only the observed apparent image, but the intrinsic intensity profile of the source can be well characterized by a Gaussian distribution. However, this may not necessarily be the case. For Sgr A*, we will show that the intrinsic intensity profile emitted by the RIAF can be quite different from the Gaussian distribution. In this case, we are unclear to the definition of the “intrinsic size”, let alone the comparison between the theoretically predicted size and the observationally derived one. Given this situation, in the present paper we will not try to calculate the “intrinsic” size of Sgr A*. Rather, we first calculate the intrinsic intensity profile from the RIAF model. Then we take into account the scatter broadening toward the Galactic center to obtain the simulated image. We will directly compare the simulated image with the observed one.

Now let’s calculate the specific intensity profile of the radiation from the RIAF. We first assume that the black hole in Sgr A* is non-rotating and the RIAF is face-on. The effects of the assumptions on the result will be discussed later. We first solve the global solution to obtain the dynamical quantities of the RIAF as stated in Section 2. Because in our calculation the Paczyński & Wiita (1980) potential is used and the calculation is in the frame of Newtonian mechanics rather than the exact general relativity (GR), the calculated radial velocity of the accretion flow very close to the black hole is larger than the speed of light thus not physical. As a result, at this region the density of the accretion flow is smaller and correspondingly the electron temperature is also lower due to weaker compression work. To correct this effect, for simplicity we compare the radial velocity obtained in our calculation with that obtained by Popham & Gammie (1998) in the frame of GR. We found that our radial velocity at $r \lesssim 30$ should be divided by $0.93e^{2.13/r}$ where r is the radius in unit of $R_g (\equiv GM/c^2)$. As for the electron temperature, following the result in Narayan et al. (1998), a correction factor of $1.4r^{0.097}$ is adopted. The above corrections are of course not precise, but fortunately the result is not sensitive to them as we will discuss in Section 4.

The resulting intrinsic intensity profiles at 3.5 and 7 mm are shown by the red solid lines in Fig. 1(b)&(f). Obviously, these two profiles can’t be well represented by a Gaussian distribution. Before we incorporate the electron scattering, however, we take into account the following additional relativistic effects, namely gravitational redshift, light bending, and Doppler boosting (Jaroszynski & Kurpiewski 1997; Falcke et al. 2000). We implement these effects using our GR ray-tracing code (Huang et al. in preparation). The dashed lines in Fig. 1(b)&(f) show the resultant intensity profiles after the above GR effects are considered. The original peak of each solid line becomes lower because of the strong gravitational redshift near the black hole. The outward movement of the peak location is due to light bending.

Fig. 1(c)&(g) show the simulated image after the scattering has been included. The scattering model mentioned at the beginning of this section is adopted. The images are elliptical, consistent with observations. The open circles in Fig. 1(d)&(h) show the intensity of the simulated image as a function of radius. The smoothness of the profile is because of the scattering broadening. The solid lines in Fig. 1(d)&(h) are Gaussian fit to the open circles. It can be seen that the intensity profile of the simulated image can be perfectly fitted by a Gaussian, as we stated above. The FWHM of the simulated images at 7 mm and 3.5 mm are $0.729_{-0.009}^{+0.01}$ mas and $0.248_{-0.002}^{+0.001}$ mas, respectively. The simulated size at 7 mm is in good agreement with the observed value by Shen et al. (2005) within the error bars but slightly larger than the observed size by Bower et al. (2004); the size at 3.5 mm is a little larger than the observation of Shen et al. (2005). Given that the size of the source may be variable (Bower et al. 2004) and the uncertainties in our calculations that we will discuss in §4, we conclude that the predictions of the YQN03 model are in reasonable agreement with the size measurements.

In the above simulation, the “input” intensity profile for the scattering simulation is the result of considering various effects or corrections. In the following we discuss the effects of these corrections by considering various “input” intensity profiles. The first profile we consider is the one without the GR effect, i.e., the red solid lines in Fig. 1(b)&(f). In this case, the FWHM of the simulated image after considering electron scattering are 0.737 and 0.239 mas at 7 and 3.5 mm, respectively. So the GR effects make the size of Sgr A* slightly larger at 3.5 mm. This is because the strong GR effects make the emission very close to the black hole weaker, while the emission at large radii almost remain unchanged. But at 7 mm, since the scattering effect is much stronger (4 times) than at 3.5 mm, the emission at both the small and large radii in the scattered intensity profile becomes weaker due to the GR effects. The total effect is that the size becomes smaller at 7 mm. We have confirmed our interpretation by simulating the image at a longer wavelength—14 mm. The second profile we consider is based on the last profiles (i.e., without considering GR effects), with the only difference that we now only consider the emission of thermal electrons in calculating the intrinsic intensity profiles. The FWHM values of the simulated image in this case are 0.724 and 0.228 mas at 7 mm and 3.5 mm, respectively. So the inclusion of the nonthermal electrons in the RIAF makes the size of Sgr A* at 7 mm and 3.5 mm larger. This is because the intensity profile from the nonthermal electrons are flatter than that of the thermal electrons. The last input intensity profile we consider is based on the second profiles above (i.e., without considering nonthermal electrons) but with the difference that the profiles of the density and electron temperature are directly obtained from the global solution of RIAF and no relativistic corrections to the profiles of density and temperature are adopted. In this case, the FWHM values of the simulated image are 0.727 mas and

0.238 mas at 7 mm and 3.5 mm, respectively. So the inclusion of relativistic corrections to the profiles of density and electron temperature makes the size of Sgr A* smaller. This is because the corrections make the emission at the innermost region of RIAF stronger.

We also calculated the simulated size of Sgr A* at 1.35 cm, which is $2.67^{+0.04}_{-0.03}$ mas. This result is consistent with the observed size of $2.635^{+0.037}_{-0.024}$ mas by Bower et al. (2004) and slightly larger than the size of $2.53^{+0.06}_{-0.05}$ mas by Shen et al. (2005). At last we try to predict an observed image of Sgr A* at a shorter wavelength—1.3 mm. The red solid line in Fig. 1(j) shows the calculated intensity profile while the dashed line is the profile after the GR effects are taken into account using the ray-tracing method. The simulated image at 1.3 mm after considering the electron scattering is shown in Fig. 1(k) and its intensity profile is shown in Fig. 1(l). Different from the cases of 7 mm (Fig. 1(d)) and 3.5 mm (Fig. 1(h)), however, the simulated intensity profile can no longer be reasonably fitted by a Gaussian (see also Fig. 1 in Falcke, Melia & Agol 2000). This indicates that the ratio between the intrinsic size and the scattering size must be larger at 1.3 mm than that at 3.5 mm where the two sizes are comparable. And as a result, the non-Gaussian distribution of the intrinsic intensity distribution significantly modulate the observed image. This prediction can be tested by future VLBI observations.

4. Summary and Discussion

The recent VLBA observations (Shen et al. 2005; Bower et al. 2004) produced high-resolution images of Sgr A* at wavelengths of 3.5 and 7 mm. The measured sizes provide a good chance of testing theoretical models. In this Letter we investigate whether the RIAF model presented in YQN03 can account for these new observations. We calculate the intrinsic intensity profile of RIAF, taking into account the relativistic corrections such as light bending and gravitational redshift. Because the intrinsic intensity profile produced by the YQN03 model can't be represented by a Gaussian (ref. the solid lines in Fig. 1(b)&(f)), we simulate the image by considering the interstellar scattering. The results are shown in Fig. 1(d)&(h). The intensity profile of such an image can be fitted by a Gaussian and we thus obtain its FWHM value and compare it directly with the observations (Fig. 1(d)&(h)). The predicted sizes of Sgr A* by RIAF model of YQN03 at 7 and 3.5 mm are $0.729^{+0.01}_{-0.009}$ mas and $0.248^{+0.001}_{-0.002}$ mas respectively, which are in reasonable agreement with observations considering the uncertainties of the calculations. We further predict an image of Sgr A* at 1.3 mm (Fig. 1 (k)&(l)) which can be tested by future observations.

In our calculations, we assume a face-on RIAF and a non-rotating black hole. If the RIAF is not face-on, the result will be more complicated, depending on the angle between

our line of sight and the rotation axis of RIAF, and the angle between the major axis of the scattering screen and the rotation axis of the RIAF. Quantitative estimation of the size in this case is thus difficult. But given the geometry of RIAF, we speculate that the results should be similar, even at the extreme case of an edge-on RIAF. If the black hole is rapidly rotating, however, the accretion flow will extend inward further compared to the case of a non-rotating Schwarzschild hole, thus the peak in the intensity profile (ref. Fig. 1(b)&(f)) will move to smaller radii and its amplitude will become higher. This will result in a somewhat smaller size of Sgr A*. Given that the predicted sizes at both 3.5 and 7 mm by the RIAF model around a Schwarzschild black hole are larger than observations, our calculations thus suggest that the black hole in Sgr A* may be rapidly rotating. The exact prediction of the angular momentum of the black hole needs fully self-consistent radiation-hydrodynamics calculations to both the dynamics and the radiation of RIAF in the Kerr geometry, which is beyond the scope of the present paper.

At last we briefly discuss the constraint of the observed size of Sgr A* on other two models of Sgr A*, namely the jet model of Falcke & Markoff (2000) and the coupled jet-ADAF model of Yuan, Markoff & Falcke (2002). One main difference between these two models associated with the present paper is that in the former the radio emission above ~ 86 GHz is produced by the nozzle of the jet while in the latter the contribution of the ADAF is significant. Falcke & Markoff (2000) calculated the size of Sgr A*. The predicted sizes of Sgr A* at 3.5 mm by the nozzle and the jet components are ~ 0.04 and 0.16 mas, respectively. Since in this model the emission at 3.5 mm is dominated by the nozzle rather than the jet, the predicted size might be $\gtrsim 0.04$ mas, much smaller than the observed value. Numerical calculations are required to confirm this speculation. On the other hand, in the jet-ADAF model, the contribution of the emission from the ADAF can dominate over that from the jet under suitable parameters. In this case, the predicted size of Sgr A* will be consistent with the observations, as we show in the present paper. Of course, the ADAF component there needs to be replaced by a RIAF, i.e., considering the outflow/convection. In that case, the main difference between the jet-ADAF model and the RIAF model is the origin of the radio emission below ~ 86 GHz.

This work was supported in part by the One-Hundred-Talent Program and the National Natural Science Foundation of China (grants 10543003 and 10573029).

REFERENCES

Aharonian, F., et al. 2004, A&A, 425, L13

Albert, J.; MAGIC collaboration 2006, ApJ, 638, L101
An, T., et al. 2005, ApJ, 634, L49
Baganoff, F. K., Maeda, Y., Morris, M. et al., 2003, ApJ, 591, 891
Bélanger, G., et al. 2004, ApJ, 601, L163
Blandford, R.D., & Begelman, M.C. 1999, MNRAS, 303, L1
Bower, G. C., et al. 2004, Science, 304, 704
Davies, R. D., Walsh, D., & Booth, R. S. 1976, MNRAS, 177, 319
Eckart, A.; Baganoff, F. K.; Morris, M. et al. 2004, A&A, 427, 1
Eckart, A. et al. 2005, submitted (astro-ph/0512440)
Falcke, H., Mannheim, K., and Biermann, P. L., 1993, A&A, 278, L1
Falcke, H. & Markoff, S., 2000, A&A, 362, 113
Falcke, H., Melia, F., & Agol, E. 2000, ApJ, 528, L13
Ghez, A. M., et al. 2003, ApJ, 586, L127
Hawley, J. F. & Balbus, S. A. 2002, ApJ, 573, 738
Jaroszynski, M. & Kurpiewski, A. 1997, A&A, 326, 419
Krichbaum, T. P., et al. 1997, A&A, 323, L17
Liu, S. & Melia, F. 2002, ApJ, 566, L77
Lo, K. Y., et al. 1985, Nature, 315, 124
Lo, K.Y., Shen, Z.-Q., Zhao, J.-H., Ho, P.T.P. 1998, ApJ, 508, L61
Manmoto, T., Mineshige, S., & Kusunose, M. 1997, ApJ, 489, 791
Marrone, D. P., et al. 2005, astro-ph/0511653
Mauerhan, J.C., Morris, M., Walter, F., Baganoff, F.K. 2005, ApJ, 623, L25
Melia, F., & Falcke, H. 2001, ARA&A, 39, 309
Melia, F., Liu, S., & Coker, R. 2001, ApJ, 553, 146
Miyazaki, A., Tsutsumi, T., & Tsuboi, M. 2004, ApJ, 611, L97
Narayan, R., Yi, I., & Mahadevan, R., 1995, Nature, 374, 623
Narayan, R. et al., 1998, ApJ, 492, 554
Narayan, R. & Goodman, J. MNRAS, 1989, 238, 963
Narayan, R. & Hubbard, W.B. 1988, ApJ, 325, 503

Narayan, R., Yi, I., & Mahadevan, R., 1995, *Nature*, 374, 623
Paczyński, B., & Wiita, P. J. 1980, *A&A*, 88, 23
Popham, R. & Gammie, C.F. 1998, *ApJ*, 504, 419
Schödel, R. et al. 2002, *Nature*, 419, 694
Schödel, R. et al. 2003, *ApJ*, 596, 1015
Shen, Z.-Q. et al. 2005, *Nature*, 438, 62
Stone, J., Pringle, J., & Begelman, M. 1999, *MNRAS*, 310, 1002
Tsuchiya, K., et al. 2004, *ApJ*, 606, L115
Yuan, F., Markoff, S., & Falcke, H., 2002, *A&A*, 383, 854
Yuan, F., Quataert, E., & Narayan, R. 2003, *ApJ*, 598, 301 (YQN03)
Yuan, F., Quataert, E., & Narayan, R. 2004, *ApJ*, 606, 894
Yusef-Zadeh, F. et al. 2006, *ApJ*, in press (astro-ph/0510787)
Zhao, J.-H., et al. 2003, *ApJ*, 586, L29

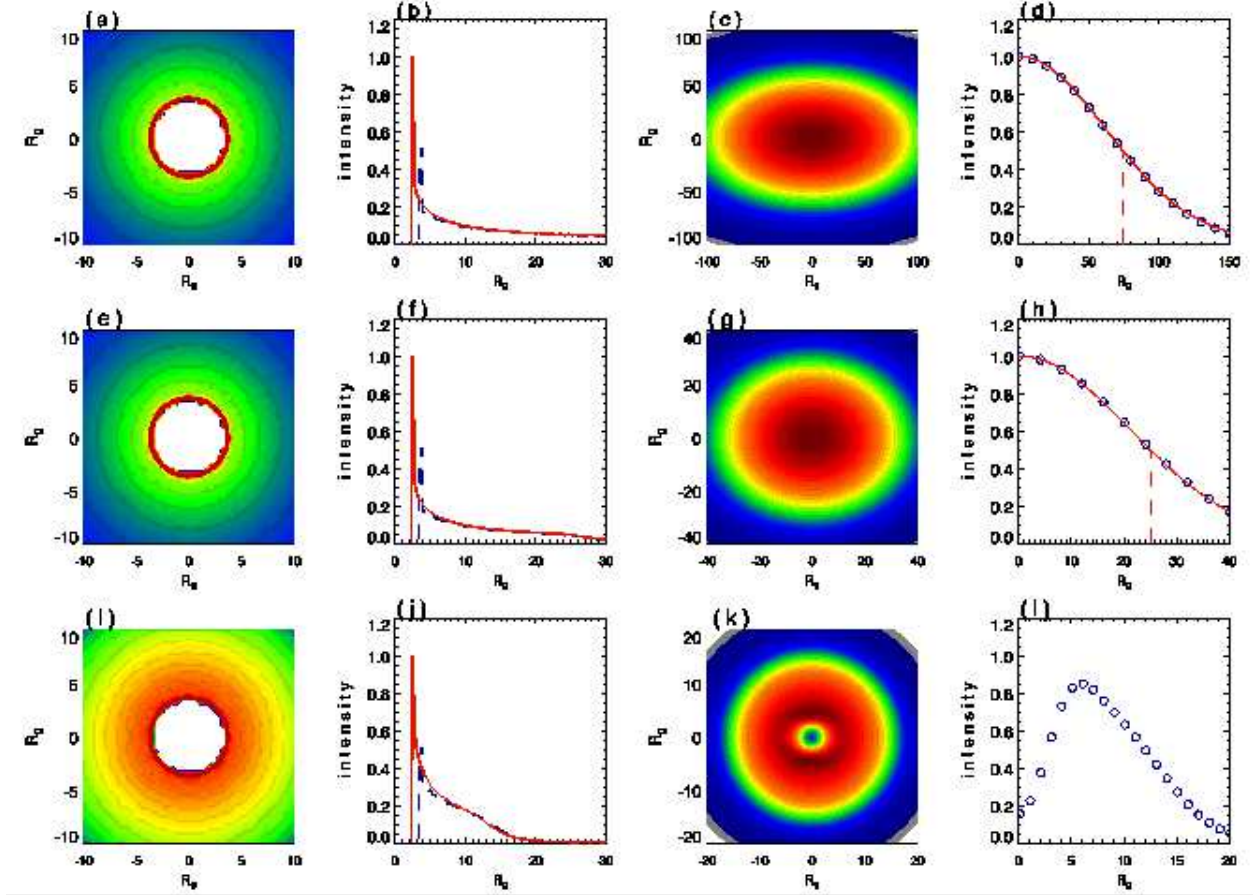


Fig. 1.— The images and sizes of Sgr A* at 7 (top panel), 3.5 (middle panel), and 1.3 mm (bottom panel). At each panel, the first column shows the “input” intensity distribution. The solid line in the second column is the intensity profile calculated from the RIAF model while the dashed line shows the intensity profile after the GR effects are taken into account using the ray-tracing method. The third column shows the simulated image after the interstellar scattering is taken into account. The open circles in the fourth column shows the intensity profile of the simulated image while the solid line shows the Gaussian fit to the circles. The vertical dashed line shows the location of the FWHM. At 1.3 mm, the simulated profile can’t be fit by a Gaussian, and thus no FWHM is indicated.